

## Integrated micro-opto-mechanical systems

Frank Merat and Mehran Mehregany

Case Western Reserve University, Department of Electrical Engineering & Applied Physics  
Cleveland, Ohio 44106-7221

### ABSTRACT

We are developing integrated micro-opto-mechanical systems (MOMS) based upon wafer integration of optical and micro-electromechanical components. In this paper, we describe our developments in micro-opto-mechanical systems in the area of microscanners and moveable optical elements. The microscanners are based upon the fabrication of micro-optical elements on the rotors of large diameter, i.e. 500 to 2000 $\mu\text{m}$ , polysilicon micromotors and have resulted in two approaches to scanning. In the first approach, nickel plating and high-aspect-ratio photolithography were used to produce 175 $\mu\text{m}$  diameter, 20 $\mu\text{m}$  tall nickel polygon reflectors on the rotors of polysilicon micromotors. These polygon microscanners are suitable for planar scanning as well and other planar applications such as optical fiber and waveguide switches. In a second approach, 2-4 $\mu\text{m}$  spatial period diffraction gratings were fabricated on the solid rotors of polysilicon micromotors. Such devices are suitable for applications requiring out-of-plane scanning, e.g., bar code readers, and take advantage of planar processing. Chemical-mechanical polishing was used to reduce the polysilicon rotor's average surface roughness ( $R_a$ ) from 420 $\text{\AA}$  to below 17 $\text{\AA}$ , improving the optical performance of the diffraction gratings. Diffraction grating microscanners using salient pole micromotors have been operated at voltages as low as 45V, with maximum operational speeds of 1100 rpm.

Although microscanners based upon rotating reflectors and diffraction gratings are significant, future MOMS will also require linear motion of optical elements and optical waveguides to carry light between optical elements. To this end, we have produced optical reflectors on linear translational comb actuators.

### 2. INTRODUCTION

Complete pre-assembled micro-opto-mechanical systems (MOMS) on silicon integrated circuits can be realized by combining Micro-Electro-Mechanical Systems (MEMS) and optics to integrate the coordinated motions of basic microactuators with optical components such as mirrors and diffraction gratings. The advantages of building an optical system in the manner of an integrated circuit is that such microfabricated MOMS: (i) will not need component alignment; (ii) can be mass produced (i.e., prices on the order of dollars per unit device); (iii) will have high packing density; (iv) can be directly integrated with electronics to produce sophisticated devices; and (v) will be small, light weight, and low power.

An example of a typical MOMS is a miniature optical scanner. Such a device could be used for a variety of applications such as bar code reading, or as optical switches for the optical fiber telecommunications industry. The development of such cheap, mass produced optical components is critical to optical fiber delivery systems into the nation's homes.

To produce micromechanical devices which can manipulate optical beams, we have developed several new micromachining processes and techniques. We have developed a new process for polysilicon surface micromachining of micromotors. We have also developed nickel plating and high-aspect-ratio photolithography processes which can be used to produce high-aspect-ratio reflective optical elements and are compatible with our polysilicon surface micromachining. Nickel surface micromachining allows us to produce optically reflective elements such as polygon reflectors on top of polysilicon micromotors or reflective sidewalls on lateral translational devices. Future development of planar MOMS will require optical waveguides for switches and duplexers. We are in the process of fabricating optical rib waveguides on silicon in a process which is compatible with our polysilicon surface micromachining.

These processing techniques have been used to fabricate basic micro-optical devices such as scanning optical mirrors and diffraction gratings which will be reported upon in detail in this paper. We are in the process of producing translatable reflectors, optical waveguide couplers, rotating optical mirrors, and diffraction gratings for MOMS devices and some preliminary devices and their performance will be reported. These devices could be used to implement optical microbenches, optical switches, and frequency-controlled lasers, as well as the scanners and other devices described in this paper.

### 3. MICROSCANNER DESIGN

Our approach to microscanners has been to integrate rotating polysilicon micromotors with micro-fabricated optical elements. This has resulted in the two approaches to scanning illustrated in Figure 1. Figure 1(a) shows a cross-sectional view of a polysilicon micromotor with a high-aspect-ratio nickel-plated polygon reflector [1,2]. This design is very similar to that of conventional polygon reflector scanners; but a microscanner implementation requires a honeycomb rotor structure and a hollow polygon to minimize the mass of the rotor and shorten the release time during processing. The rotating optical reflector of this

design is particularly suited to in-plane motion of an optical beam for such devices as optical waveguide switches and planar scanning applications. To address different applications which require scanning out of the plane of the substrate, a micromotor which incorporates a rotating optical diffraction grating fabricated on top of the rotor can be used as shown in Figure 1(b). Such rotating diffraction grating devices, which can operate in a transmissive or reflective mode depending upon the substrate material, can rapidly scan a laser beam in a repeatable pattern out of the plane of the substrate.

Experimentally, the devices of Figure 1(b) exhibit less diffraction than the polygon reflector of Figure 3(a) because much larger optical elements are being used for reflection, i.e., a motor radius of  $\sim 250\mu\text{m}$  as compared to the  $20\mu\text{m}$  tall sidewall of a nickel plated reflector. These are typical dimensions which are achievable with the processing techniques described in the following section.

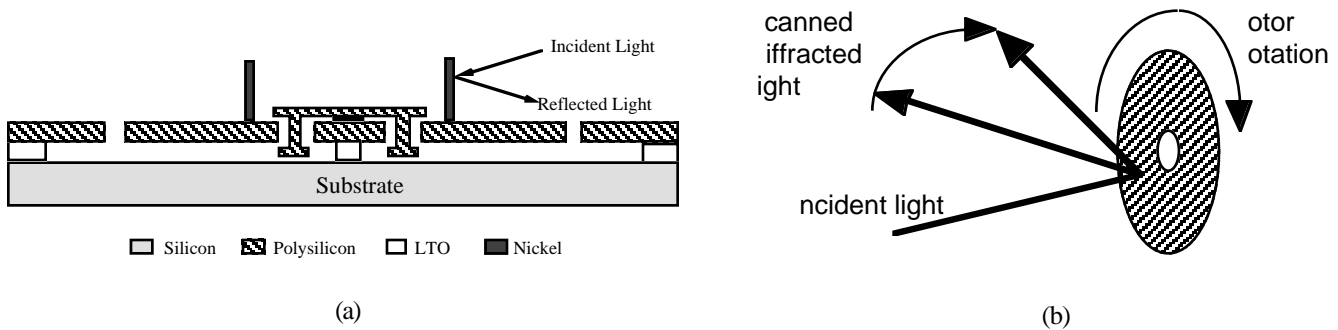


Figure 1. Polysilicon micromotor scanner operation using (a) metallic polygon and (b) diffraction grating fabricated on the rotor of the micromotor.

### 3.1 Polygon Microscanners

A planar view of a polysilicon microscanner consisting of a hollow, nickel plated polygon reflector on the rotor of an electrostatic drive micromotor is shown in Figure 2. The nickel plated polygon reflector is approximately  $175\mu\text{m}$  in diameter,  $20\mu\text{m}$  tall, and  $10\mu\text{m}$  thick. The diameter of the micromotor rotor is  $500\mu\text{m}$ . These dimensions are typical of microscanners produced by the processing described in the next section. The  $20\mu\text{m}$  vertical height of the nickel reflector is typical of elements that can be produced by our nickel plating process. We have produced micromotor scanners similar to Figure 2 with diameters from  $250$  to  $1000\mu\text{m}$  although the larger micromotors do not operate reliably after release.

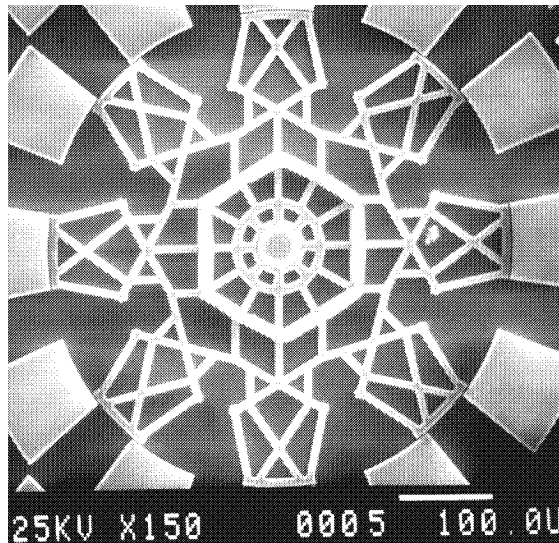


Figure 2. SEM photo of a rotating polygon optical microscanner made by electroless-plating of nickel reflecting surfaces on the rotor of a  $500\mu\text{m}$  diameter salient-pole micromotor. The thickness (height) of the nickel is  $20\mu\text{m}$ ; the width of the nickel is  $10\mu\text{m}$ . The polygon itself is approximately  $175$  microns in diameter.

### 3.2 Diffraction Grating Microscanners

An optical microscanner which consists of a diffraction gratings on the rotor of an electrostatic polysilicon micromotor is shown in Figure 3. Such microscanners have been produced with uniform gratings over the entire rotor, as well as with pie-shaped (pyramidal) radially-oriented diffraction grating elements as shown in Figure 3. The diffraction grating microscanners produced had diffraction grating spatial periods from 2 and  $4\mu\text{m}$ . This lower limit was determined by the approximate  $1\mu\text{m}$  spatial resolution of our photolithography process. It is important to note that the micromotors rotors are solid, with no release holes, allowing the production of high-quality diffraction gratings.

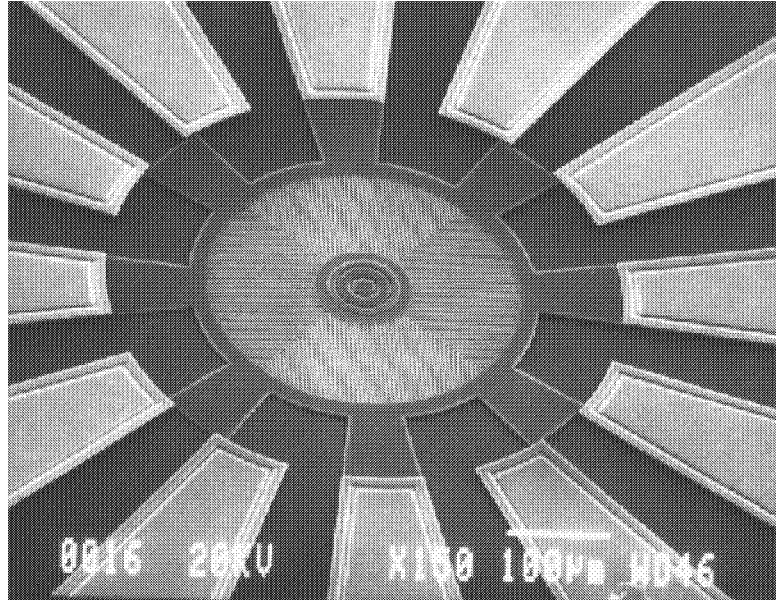


Figure 3. SEM photo of a rotating diffraction grating microscanner. The motor is a  $500\text{-}\mu\text{m}$  diameter salient-pole side-drive micromotor with polished polysilicon rotor/stator and four pyramidal grating elements with  $1.8\mu\text{m}$  spatial period.

## 4. PROCESSING

The development of MOMS requires that different optical and mechanical devices be produced on a common silicon substrate. This requires that the associated processing technologies be compatible. The basis of our MOMS processing is a simple polysilicon surface micromachining process which was developed to produce micromotors quickly and with low processing complexity [3]. Using this process, flange bearing millimeter-sized wobble and salient-pole micromotors have been produced which are the largest side-drive, polysilicon surface micromachined electrostatic motors reported to date. Typical dimensions for these motors are rotor diameters of  $500$  to  $1000\mu\text{m}$ , rotor/stator gaps of  $1.5$  to  $2.5\mu\text{m}$ , and rotor/stator thicknesses of  $5\mu\text{m}$  [3]. These millimeter sized micromotors operate smoothly and reproducibly in room air for extended periods after release. Minimum operating voltages can be as low as  $12\text{V}$ , while maximum rotor speeds have been limited by the power supply to  $2500$  rpm for microscanners fabricated on milli-sized salient-pole motors and  $1000$  rpm for microscanners fabricated on milli-sized wobble motors. These milli-sized motors have motive torques over an order of magnitude larger than previously reported polysilicon micromotors. Experimental gear ratios have been measured as a function of excitation voltage for loaded (e.g., nickel plated) and unloaded (e.g., unplated) wobble motors. As expected, the gear ratio increases with increased load. An increase in the gear ratio at the smaller excitation voltages (and hence smaller motive torques) is due to increased rotor slip.

Photolithographic techniques for producing high aspect ratio structures have been developed and successfully used to produce a minimum linewidth of  $3.5\mu\text{m}$  and a line spacing of  $2.5\mu\text{m}$  in  $23\mu\text{m}$  thick photoresist (corresponding to an aspect ratio of  $7.7$ ). This process has been used with an electroless nickel plating in the nickel surface micromachining process described below to fabricate high-aspect-ratio nickel reflective structures on polygon microscanners as well as on linear actuators. A process for producing rib optical waveguides which is compatible with micromachining processing is under development and test devices are currently being fabricated.

### 4.1 High-aspect-ratio photolithography

We have developed a high-aspect-ratio photolithography process using a positive photoresist of high viscosity and high transparency, and standard UV light exposure [4]. In this process, the wafers undergo a dehydration bake and HMDS (hexamethyldisilazine) vapor prime in a HMDS oven at  $150^\circ\text{C}$ . A thick photoresist (Hoechst, AZ 4620) is then spin-coated at

2000 rpm. Edge bead removal is performed to ensure a smooth photoresist surface. The wafers are then pre-baked at 95-100°C for 30 minutes in a convection oven. The wafers undergo an additional coating, edge bead removal, and pre-bake under the same conditions to give a photoresist layer that is approximately 20µm thick. The wafers are then aligned using a contact aligner with a standard UV light source. The plating molds are formed after development in an alkaline developer (Hoechst, AZ-400K) diluted in de-ionized water. The photoresist is usually postbaked after exposure to improve both adhesion of the photoresist to the substrate and chemical resistance of the photoresist. By eliminating this postbake and the consequent mold distortions, mask features (with steep side walls) as small as 2µm were achieved in 20µm thick photoresist.

#### **4.2 Nickel surface micromachining**

A surface micromachining process, which we call nickel surface micromachining, has been developed for the fabrication of metallic electrostatic microactuators [5,6]. This process uses a nickel structural layer which is directly deposited on a polysilicon sacrificial layer by electroless nickel plating without the need for a metallic seed layer. This process can be used with high-aspect-ratio photolithography described in the previous section to produce tall (e.g., 20µm or greater) microstructures with reflective sidewalls. We have also used it to produce electrically conductive such as electrical microrelays [6]. The process consists of four steps: (i) deposition of electrical isolation and sacrificial layers; (ii) fabrication of the plating mold by high-aspect-ratio photolithography; (iii) deposition of the nickel by electroless plating; and (iv) release of the plated devices. This process can be described in detail as:

##### Deposition of isolation and sacrificial layers

Starting with a (100) silicon wafer, a 0.5µm to 1µm thick oxide layer is thermally grown at 950°C. This oxide layer is used for electrical isolation of the substrate and also protects the substrate during the initial device release step in KOH. Next, a 2.5µm to 5µm thick undoped polysilicon layer is deposited at 600°C by LPCVD. This polysilicon film acts as a plating and sacrificial layer for the subsequent electroless plating of nickel microstructures. The thickness of the polysilicon has been shown to affect the surface roughness of the subsequently plated nickel film, with thicker polysilicon films resulting in nickel films with larger values of surface roughness.

##### Fabrication of the plating mold

For the plating mold features defined in photoresist, large height-width aspect ratios, vertical sidewalls, and material compatibility with plating chemicals are desirable. To meet these objectives, we have developed and used a high-aspect-ratio photolithography process to produce features as small as 2µm in 20µm thick photoresist with steep sidewalls [4].

##### Deposition of nickel by electroless plating

Prior to plating, the polysilicon surface to be plated is pretreated by an acid etch, followed by a 2-3 minute deposition of palladium as a starting catalyst, and a final acid etch to remove any tin oxide. This pretreatment causes the polysilicon surface to become rough, providing mechanical bonding sites for adhesion of the nickel to the polysilicon. The etch rate and surface morphology of polysilicon vary depending upon the polysilicon grain size which, in turn, depends upon the LPCVD deposition conditions. Very short etch times do not uniformly initiate the nickel plating; long etch times reduce the polysilicon film thickness significantly, reducing the mechanical integrity of the nickel film.

##### Release

The etched devices are released by selectively etching the polysilicon layer from everywhere but the anchor regions under the plated nickel. We use a timed etch of the polysilicon using 40 wt.% KOH at approximately 6µm/hour.

#### **4.3 Micromotor Fabrication**

Polysilicon surface micromachining has been used to fabricate the largest (500-2000µm) side-drive, polysilicon surface micromachined electrostatic motors reported to date [7]. These large diameters have been motivated by the typical dimensions of optical micro-devices, i.e., hundreds of microns, necessary to minimize optical diffraction, and by the accompanying size of the motors or linear actuators needed to move such micro-optical elements.

The micromotors for the polygon microscanner were fabricated by a modification of our three mask processing [7]. The rotor, stator and bearing were fabricated from heavily phosphorous-doped polysilicon. LTO was used for substrate/stator isolation, as well as the sacrificial layer under the rotor. The bearing clearance was produced by thermal oxidation. A thick (10-20µm) photoresist layer was spun cast and patterned to make the mold for nickel plating. Nickel was deposited by the process described above and the mold removed. The rotors were then released in HF for approximately 10 minutes with no alteration of the reflective properties of the nickel. The rotors were patterned in a honeycomb pattern to reduce the mass of the rotor while providing rigid support for the nickel plated optics.

The micromotors for the diffraction grating microscanner were designed with a large, solid rotor without release holes as a base upon which to fabricate optical elements. The large rotor diameter necessary for the scanner required thick (e.g., 5.5µm) polysilicon rotor/stator films to provide sufficient mechanical stiffness and to prevent out-of-plane warping of the large area rotor.

However, with increasing LPCVD polysilicon thickness, the film roughness increases. Longer diffusion times are also needed to subsequently dope the polysilicon, further increasing the surface roughness. This inherent polysilicon surface roughness results in two limitations: (i) feature size definition and quality degradation; and (ii) for optical applications, undesirable optical scattering which were overcome by using chemical-mechanical polishing (CMP) as described in the following section. The complete fabrication process is illustrated schematically in Figure 4. A 450 nm nitride layer (for electrical isolation) is laid down on top of a (100) silicon wafer. A 3.5 $\mu\text{m}$  PSG layer is then deposited and patterned for the rotor and stator. Note the presence of anchors for the rotor bearing and stator at the end of step (a). This was necessary to prevent the rotor and stator from floating away during the long release. A 5.2 $\mu\text{m}$  thick LPCVD polysilicon layer was then deposited, followed by heavy phosphorous doping. CMP was used to produce a smooth rotor surface for the grating formation. The grating was patterned and etched by an isotropic dry etch to approximate a sinusoidal grating profile. The rotor and stator were then defined and etched by a highly anisotropic dry etch to produce the 1 $\mu\text{m}$  rotor/stator gaps. The flange mold is then defined and etched followed by a 0.3 $\mu\text{m}$  bearing clearance oxidation. A 1 $\mu\text{m}$  thick polysilicon layer is deposited by LPCVD and patterned to produce the bearing.

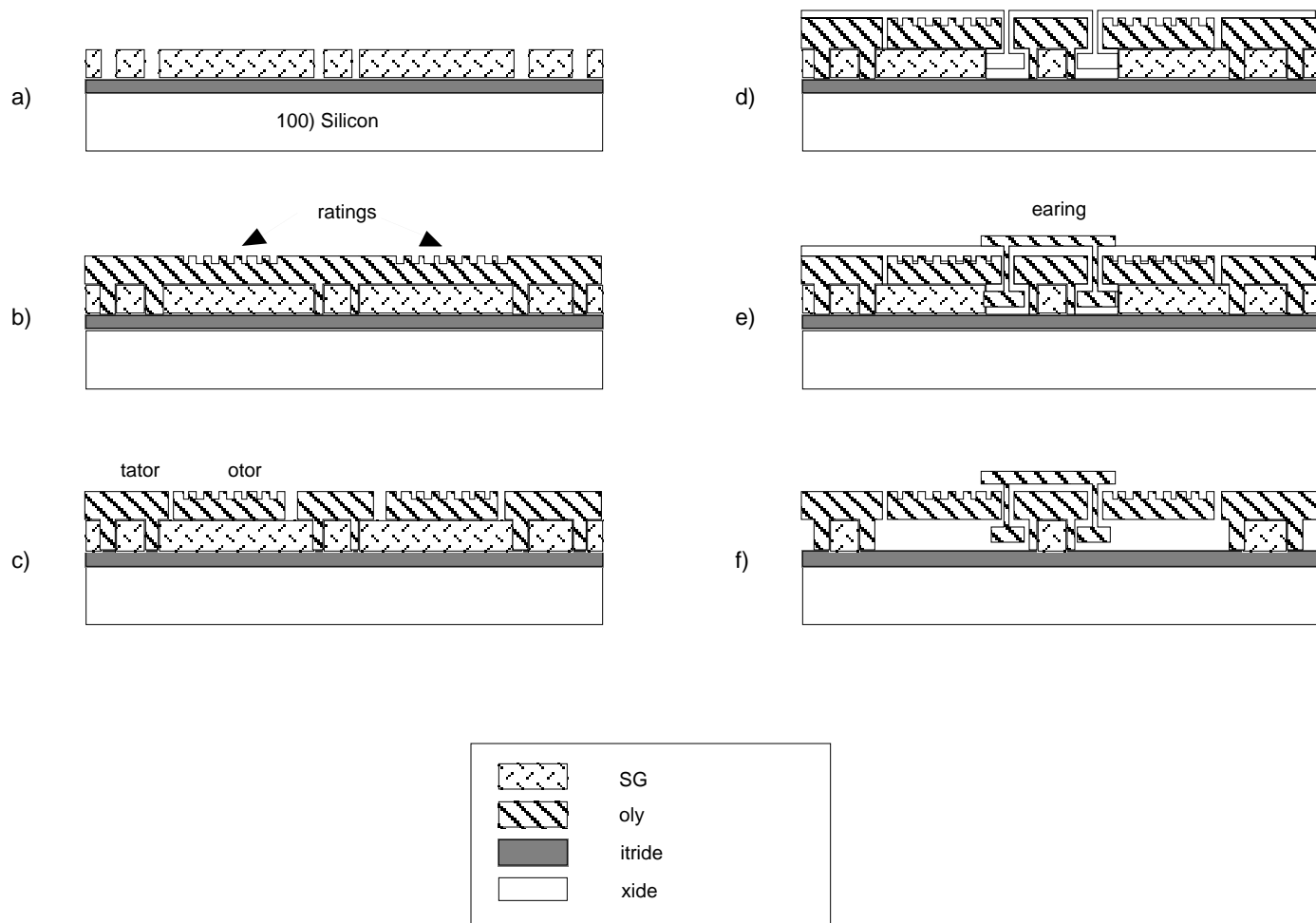


Figure 4. Cross-sectional schematics describing the fabrication process for a solid rotor, grating micromotor scanner: (a) anchor definition and patterning; (b) grating definition and patterning; (c) rotor/stator definition and patterning; (d) bearing clearance oxidation; (e) bearing definition and patterning; and (f) released device. Polishing of the wafer surface and subsequent patterning occurs between step (a) and (b).

#### 4.4 Chemical-mechanical polishing (CMP)

The fabrication of optical elements such as mirrors and diffraction gratings requires that the average surface roughness ( $R_a$ ) be low. Diffraction gratings also impose stringent line width and spacing control requirements during photolithography and pattern delineation for satisfactory optical performance. To meet these requirements, CMP was used on the polysilicon rotor

surface prior to fabrication of the diffraction grating or other optical elements. By optimizing the pressure, pad roughness, the pad/wafer speed, and the pH, particle size, and solids content of the slurry, the average polysilicon surface roughness ( $R_a$ ) of the 5.5 $\mu\text{m}$ -thick polysilicon films for the rotor of the diffraction grating microscanner was reduced by over an order of magnitude. The surface roughness ( $R_a$ ) was measured to be 420 $\text{\AA}$  before CMP to below 17 $\text{\AA}$  (with less than 1500  $\text{\AA}$  film removal) after CMP.

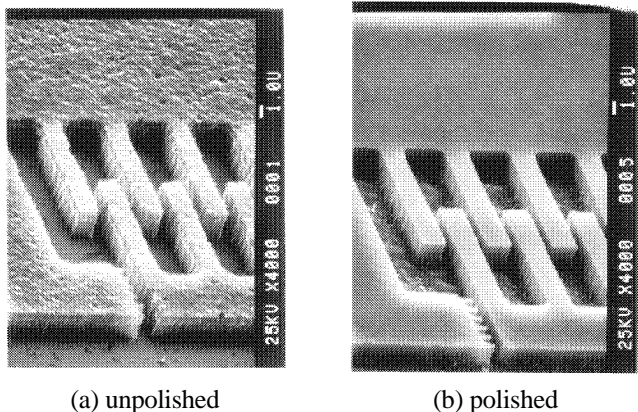


Figure 5. Close-up view of test structures in 3.5 $\mu\text{m}$  thick polysilicon showing improved feature definition, side wall quality, line width resolution, and polysilicon surface roughness achieved with CMP.

Figure 5 demonstrates the significant feature size definition and quality (e.g., sidewall smoothness) improvement, as well as the substantial surface roughness reduction, achieved with CMP on a test structure. Figure 5 shows the same test structure but with no CMP used in the fabrication of the structure shown in 5(a) and CMP used to fabricate the structure shown in Figure 5(b). Note especially the ruler which is almost invisible in the foreground of Figure 5(a) is clearly defined in Figure 5(b) demonstrating the increase in resolution achieved with CMP. Figure 6 shows diffraction gratings fabricated with and without CMP.

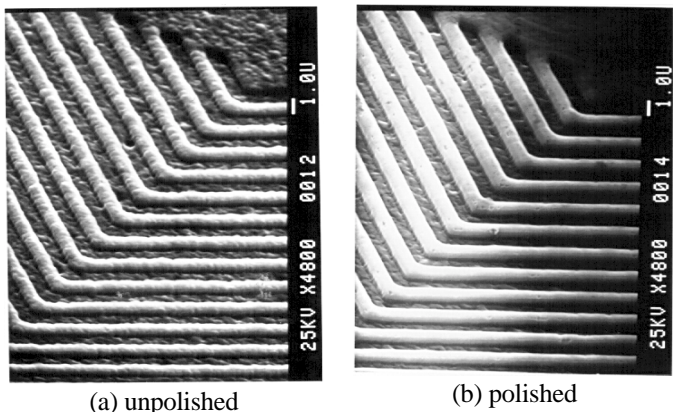


Figure 6. Close-up view of 2 $\mu\text{m}$  spatial period diffraction gratings produced on thick polysilicon showing improved feature definition, side wall quality, line width resolution, and polysilicon surface roughness achieved with CMP.

## 5. RESULTS

### 5.1 Polygon Microscanners

Optical testing of polygon microscanners was done on a 500 $\mu\text{m}$  diameter wobble micromotor with a 175 $\mu\text{m}$  diameter, 20 $\mu\text{m}$  tall nickel plated polygon reflector on the rotor. The incident light came from a multi-mode optical fiber (illuminated by a 633 nm He-Ne laser) positioned just above the plane of the substrate and just beyond the rotor/stator gap. Using this illumination, the reflected beam shown in Figure 7(a) was measured approximately 10 inches from the micromotor with an ordinary camcorder. The vertical fringes in Figure 7(a) appear to be caused by optical reflections from the rotor surface rather than from diffraction of the optical beam by the polygon. The effect of these reflections is to create a “noisy” signal as shown in photodiode measurements of the reflected signal as shown in Figure 7(b). The low frequency variation of the reflected light in Figure 7(b) is hypothesized to be a low frequency wobble of the rotor about the axis of rotation.

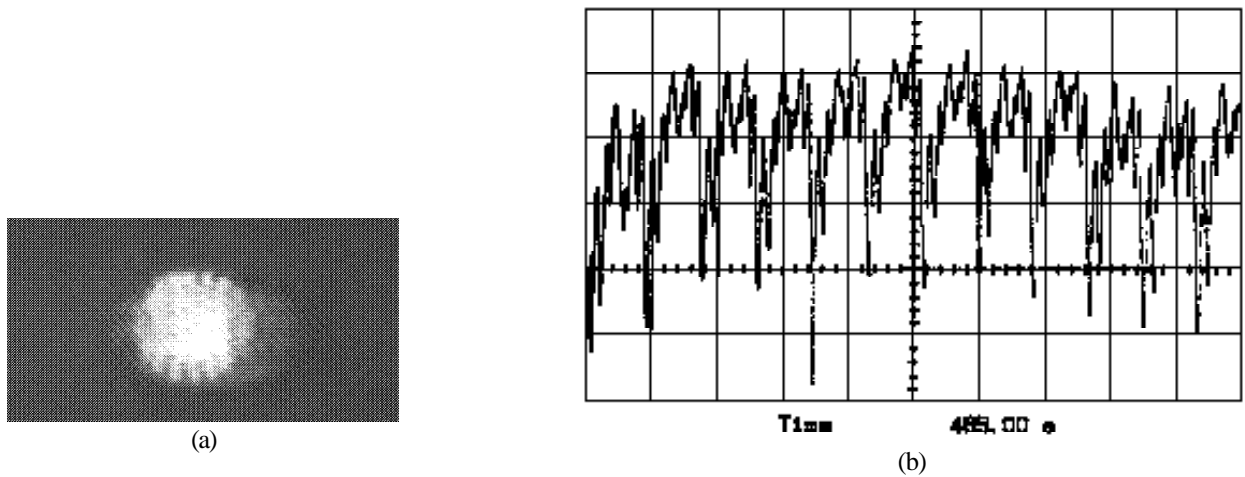


Figure 7. Reflected laser radiation from a 175 $\mu\text{m}$  diameter, 20 $\mu\text{m}$  tall nickel plated polygon on a rotating micromotor operated at constant low speed and illuminated by 633 nm radiation from a multi-mode fiber slightly above the plane of the rotor. (a) Video image of the reflected spot recorded using an ordinary television. (b) Photodiode measurements of the reflected spot. The complex shape of the reflection is caused by undesired reflections from the rotor. All measurements were made approximately 10 inches from the scanner.

## 5.2 Diffraction Grating Microscanners

Optical testing of the diffraction grating microscanner was done using 2 and 4 $\mu\text{m}$  period gratings fabricated on the 500 $\mu\text{m}$  diameter rotor of a salient pole polysilicon micromotor. The nominally (i.e., as designed) 2 and 4 $\mu\text{m}$  grating periods were measured (from the diffraction of a 633 nm He-Ne laser beam) to be 1.80 and 3.86 $\mu\text{m}$ , respectively. The diffraction orders for the 1.80 $\mu\text{m}$  gratings illuminated by a He-Ne laser were separated by  $20.79^\circ \pm 0.62^\circ$  and those for the 3.86 $\mu\text{m}$  gratings by  $9.8^\circ \pm 0.53^\circ$ . The difference between design and experimental grating periods is attributed to variations in timed etching and photolithography. The grating etch depth can be adjusted to maximize intensity in a desired diffraction order (e.g., typically the first order) for a given incident optical wavelength.

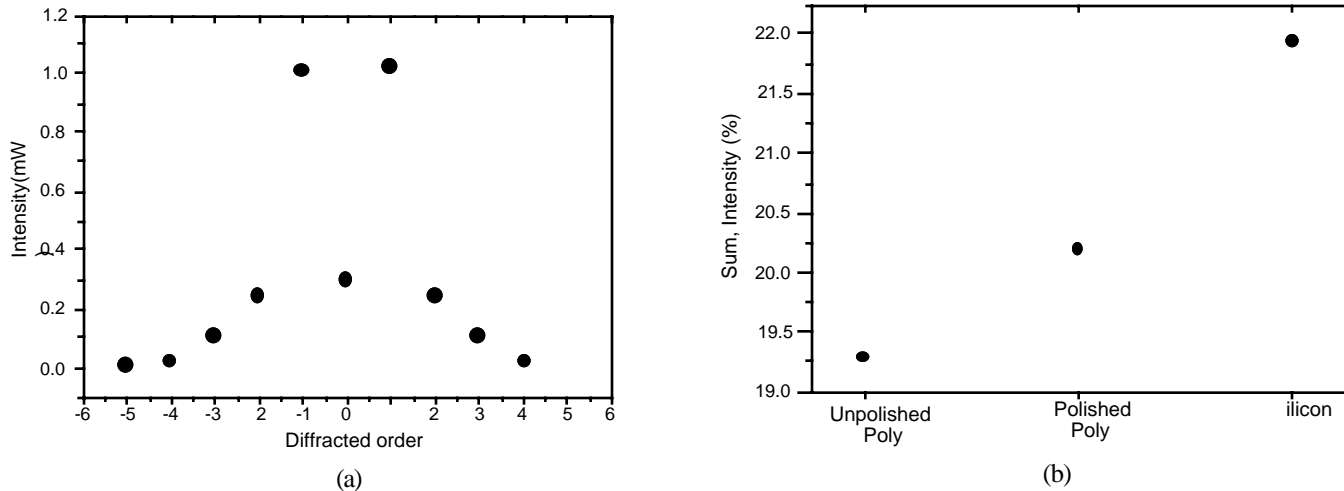
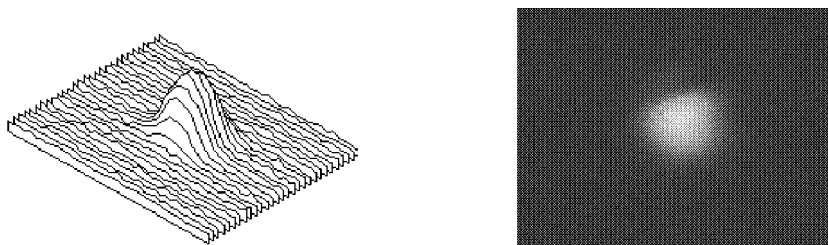


Figure 8. Optical measurements of diffraction gratings. (a) Distribution of optical energy among diffraction orders for a 3.86 $\mu\text{m}$  period grating in polished polysilicon. (b) Total optical energy (all diffraction orders) from gratings fabricated on polished and unpolished polysilicon, as well as single-crystal silicon wafers.

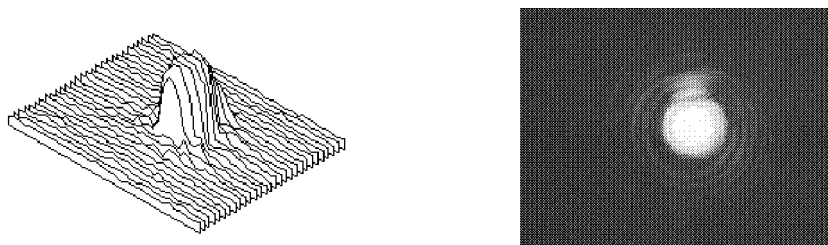
Figure 8(a) shows the measured optical power of the various diffraction orders from a 2 $\mu\text{m}$  period, 500 $\mu\text{m}$  diameter uniform diffraction grating. Note that the first order power is clearly dominant as would be expected of an approximately sinusoidal grating profile. Adjusting the grating etch depth can be used to shift power from the first order to higher diffraction orders. The

importance of polishing the optical rotor surface prior to fabricating the diffraction grating is shown in Figure 8(b). The total diffracted power (sum of measured power of all diffraction orders) was measured for 2 $\mu\text{m}$  period test gratings fabricated in unpolished polysilicon, polished polysilicon, and single-crystal silicon. The total diffracted power is expressed as a fraction of the incident power. For reference, note that the reflected power from a polished silicon wafer (with no grating) would be approximately 30%.

The diffracted beams were characterized by illuminating the entire grating by a He-Ne laser beam and measuring the diffracted beam profiles with a CCD camera. All diffraction orders provided nearly Gaussian beam profiles, with the gratings on polished polysilicon producing a higher degree of spatial uniformity and lower beam divergence than those on unpolished polysilicon. Figure 9 compares measured beam profiles on polished and unpolished polysilicon 2 and 4 $\mu\text{m}$  period at a distance of 1m from the microscanner. The grating periods and diffraction angles were uniform for similar gratings on the same wafer and between different wafers. Optical scanning at distances up to several meters without external optics is readily achievable. The effects of small (0.5 mm diameter) motor diameter were found to be negligible upon the overall optical performance of the diffraction grating microscanner. No diffraction from the 500 $\mu\text{m}$  diameter rotor was seen in the beam profiles. Diffraction from the 25 $\mu\text{m}$  radius bearing is seen as a circular diffraction pattern in the beam profile of Figure 9 (b).



(a) Beam intensity profile (left) and spot quality (right) from gratings fabricated on unpolished polysilicon.



(b) Beam intensity profile (left) and spot quality (right) from gratings fabricated on polished polysilicon

Figure 9. Beam intensity profiles and spot quality from similar gratings fabricated on (a) unpolished and (b) polished polysilicon rotors. The profiles were taken at 0.5 meter distance from a grating microscanner using 633 nm light. Note the increased intensity and reduced beam divergence as a result of polishing.

The diffraction grating microscanners designed in this paper operated smoothly and reproducibly in room air for extended periods after release. Super-critical CO<sub>2</sub> [1] release was needed to permit the scanners to operate without stiction after release. Both 1 and 2 $\mu\text{m}$  rotor/stator gap motors are operational. Minimum operating voltages are as low as 45V, while maximum rotor speeds have been as high as 1100 rpm (limited by the driving electronics) for the salient-pole micromotor design and 23 rpm for the wobble micromotor design. Larger diameter grating microscanners were produced but have not been found to operate reliably.

Scanning of a laser beam was demonstrated using a 633 nm He-Ne laser to illuminate a uniform 1.80 $\mu\text{m}$  period, 500 $\mu\text{m}$  diameter grating on a salient-pole micromotor. The scanned beams were detected with a silicon photodiode and recorded with a dynamic digital signal analyzer over many revolutions of the scanner. Figure 10 shows a typical intensity profile for a salient-pole microscanner during operation indicating the high repeatability and uniformity of the scanner operation over extended periods of time.

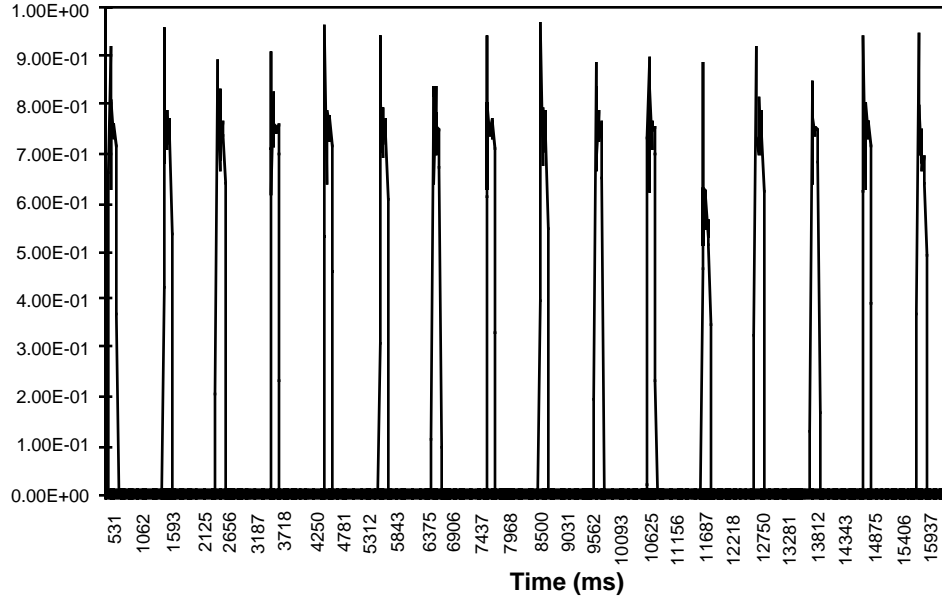
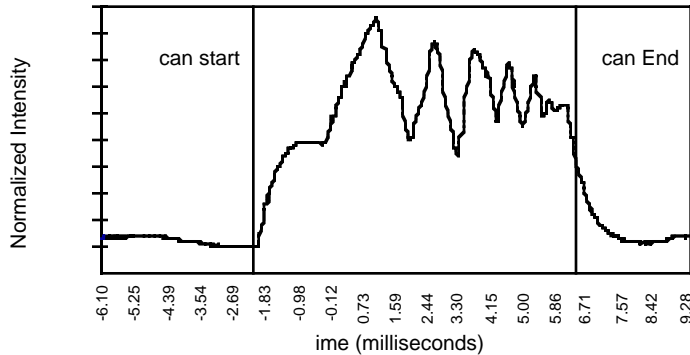


Figure 10. Typical scan intensity measured over several revolutions of the micromotor scanner. The 500 $\mu$ m-diameter salient-pole microscanner is turning at 60 rpm.

### 5.3 Typical Bar Code Scanning Application

We have demonstrated bar code scanning using a grating microscanner. The simple test bar code, shown in Figure 11(a), is illuminated by a laser beam diffracted by the grating microscanner. Figure 11(b) displays a typical photodiode signal resulting from scanning a 633 nm He-Ne laser beam over the bar code pattern. The optical reflection from the bar code is detected by a silicon photodiode and a digital dynamic signal analyzer. No external lens system is used in the experiment with the grating microscanner. The peaks and valleys in the trace correspond to the light and dark areas of the bar code. The shape of this trace is dependent on many factors including motor speed, light intensity, relative positions of the bar code detector, detector acceptance angle, and detector time constant. The detected signal can be improved by external optics to suit the requirements of many commercial bar code reading applications.



(a) Test bar code with alternating light and dark periods with decreasing bar width and spacing

(b) Reflected signal from the test bar code in (a) using a grating microscanner illuminated by a He-Ne laser

Figure 11. Demonstration of bar code reading using a diffraction grating microscanner. Note that the signal peaks correspond to the light areas and the valleys correspond to the dark areas of the bar code.

## 6. LATERAL TRANSLATIONAL REFLECTORS

We are also developing a lateral translating reflector using the same basic processing as used for the rotating polygon scanner. A three-mask design for the linear translatable reflector was developed, and our nickel surface micromachining process was used to fabricate the device shown in Figure 12. We have obtained released nickel plated features with lengths of 500 $\mu$ m and

20 $\mu$ m thickness. The mechanical properties of these thin nickel films are being determined, and preliminary experiments show that the nickel films are being deposited in a state of very low tensile stress [8]. The nickel microactuator devices are currently undergoing detailed mechanical and optical testing. Such translational mirrors could be used in interferometers and/or for tuning laser diodes.

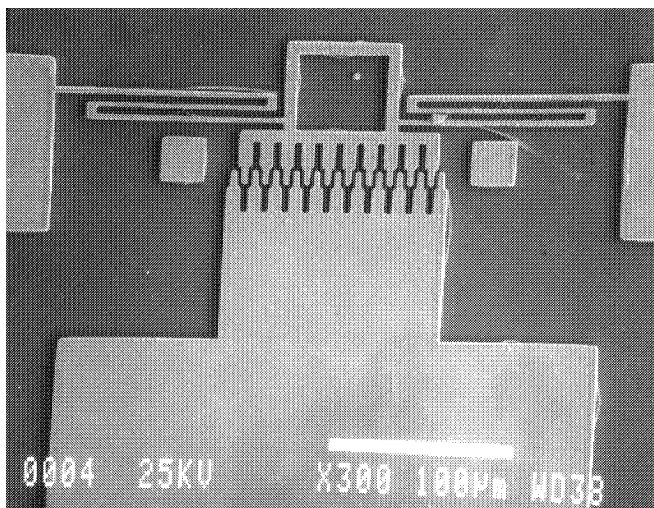


Figure 12. Electrostatic drive lateral translational reflector. Note that the sidewall of the surface at the top center of the image is nickel plated and will be used as an optical reflector.

We plan to improve the nickel plating and silicon machining processes by characterizing and measuring the variation of lines/spaces with film thickness, variation of side wall with thickness, variation in stress with thickness, the optical characteristics of plated reflectors, and the effects of annealing. This information will be used to decrease the surface roughness of plated surfaces, increase the uniformity of the plating process, and optimize the release process.

## 7. DISCUSSION & CONCLUSIONS

We have used MEMS technology to develop polysilicon surface micromachining, nickel surface micromachining, chemical-mechanical polishing and high-aspect-ratio lithography. Nickel surface micromachining has been used to produce metallic microstructures with optical quality sidewalls on rotating and linearly translatable polysilicon devices. We are developing a process for fabricating optical waveguides which is compatible with our polysilicon and nickel surface micromachining processes. These processes can be combined to produce basic micro-opto-mechanical devices, e.g., rotating polygon reflectors, rotating diffraction gratings, and translatable reflectors. These devices can be utilized individually or in combination to fabricate miniature optical scanners, optical interconnects, optical duplexers or other devices. We have demonstrated polygon and diffraction grating microscanners and have used a grating microscanner to read a bar code. MOMS are extremely small in size, allowing innovative applications. Complex MOMS which incorporate cantilever beam scanners and microlenses, micromotor scanners, and micro-reflectors on linear translators appear to be achievable. Free space optical switches utilizing salient pole diffraction grating microscanners appear to be a very natural extension of our present developments and will be pursued.

MOMS may be critical to practical implementation of optical fiber subscriber loops for telecommunications. In particular, such systems may require optical microbenches that permit low-cost manufacture of pre-aligned, hybrid fiber optic systems (e.g., transmitters and receivers), optical fiber switches, and frequency modulated and/or controlled diode lasers. The development of complex MOMS will require more attention to process integration and continued pursuit of waveguide and other technologies which are compatible. Our optical duplexer development is a realistic development in demonstrating the integration micromachining processing. We are presently developing optical switches using salient pole diffraction grating microscanners and free space modes. Our diffraction gratings microscanners show that large-area diffraction gratings can be successfully integrated with microactuators. Such large microfabricated diffraction gratings, integrated with a suitable actuator, might be used to tune the frequency of a diode laser. We plan to continue our development of micro-optical devices which incorporate moveable diffraction gratings

## 8. ACKNOWLEDGMENTS

The authors wish to acknowledge the work of our many excellent graduate students (especially S. Smith, S. Roy and A.A. Yasseen), our postdoctoral students, and visiting scientists who have performed much of the experimental work described in this paper. This work has been partially supported by ARPA under grant FQ8671-9301675, and by the Reliance Electric Corporation.

## 9. REFERENCES

1. H.Miyajima, K.Deng, M.Mehregany, F.L.Merat, and S.Furukawa, "Fabrication of Polygon Mirror Microscanner by Surface Micromachining," Proceedings SPIE, Volume 2291, Integrated Optics and Microstructures II, 1994.
2. K. Deng, H. Miyajima, V.R Dhuler, M. Mehregany, S.W. Smith, F.L. Merat, and S. Furukawa, "The Development of Polysilicon Micromotors for Optical Scanner Applications," presented at 1994 Solid-State Sensor and Actuator Workshop, Hilton Head, South Carolina, June 1994.
3. K.Deng, M.Mehregany, and A.S.Dewa, "A Simple Fabrication Process for Side-Drive Micromotors," Technical Digest, 7th International Conference on Solid-State Sensors and Actuators (Yokohama, Japan, June 1993), p. 756-759.
4. H. Miyajima and M. Mehregany, "High-Aspect-Ratio Photolithography for MEMS Applications," submitted to J. Micromechanical Systems.
5. S. Furukawa, S.Roy, H. Miyajima, Y. Uenishi and M. Mehregany, "Nickel Surface Micromachining," Proceedings, Microstructures and Microfabricated Systems Symposium, at the 185th Electrochemical Society Meeting, San Francisco, California, May 22-27, 1994, pp. 38-46.
6. S. Roy and M. Mehregany, "Fabrication of Electrostatic Nickel Microrelays by Nickel Surface Micromachining," presented at 1995 MEMS Workshop, Amsterdam, Netherlands.
7. A.A. Yasseen, S.W. Smith, M. Mehregany and F.L. Merat, "Diffraction Grating Scanners Using Polysilicon Micromotors," presented at 1995 MEMS Workshop, Amsterdam, Netherlands.
8. S. Roy, S. Furukawa, H. Miyajima, and M. Mehregany, "*In Situ* Measurement of Young's Modulus and Residual Stress of Thin Electroless Nickel Films for MEMS Applications," presented at Materials Research Society Fall Meeting, Boston, MA, 1994.